ACS APPLIED ENERGY MATERIALS

www.acsaem.org Article

In Situ Synthesis of Polythiophene and Silver Nanoparticles within a PMMA Matrix: A Nanocomposite Approach to Thermoelectrics

José F. Serrano-Claumarchirant,[§] Alvaro Seijas-Da Silva,[§] Juan F. Sánchez-Royo, Mario Culebras, Andrés Cantarero, Clara M. Gómez,* and Rafael Abargues*

Cite This: *ACS Appl. Energy Mater.* 2022, 5, 11067−11076 Read Online

ACCESS | Metrics & More | Article Recommendations | Supporting Information

ABSTRACT: The processability of organic thermoelectric materials plays a crucial role due to their clear advantages of applicability in large-scale areas compared to traditional inorganic counterparts. A promising way to process thermoelectric materials based on conductive polymers is through in situ polymerization in an insulating polymer matrix. This work shows an interpenetrating polymeric network based on polythiophene, silver nanoparticles (Ag NPs), and poly(methyl methacrylate) (PMMA) produced by the oxidative polymerization of terthiophene by an oxidizing silver salt in a PMMA matrix. Ag NPs are in situ synthesized simultaneously as a byproduct. The reaction occurs very fast in the solid state, and after only 1 min, a homogeneous interpenetrating polymer network (IPN) film is obtained, reaching electrical conductivity values of 120 S cm^{-1}. Ag NPs play a determining role in the conducting properties of the IPN. Moreover, the thermoelectric properties were evaluated as a function of the synthesis parameters, reaching a maximum power factor of 51 $\mu W\ m^{-1}\ K^{-2}$. This study shows a promising method to enhance the processability of hybrid thermoelectric materials on the basis of conductive polymers and nanofillers.

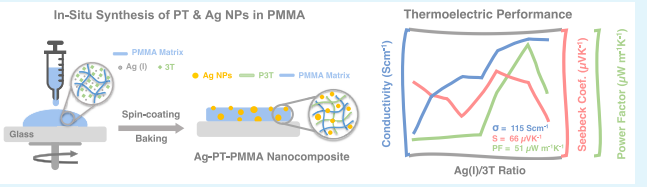

KEYWORDS: *in situ synthesis, conducting polymer, silver nanoparticles, thermoelectric materials, thin films*

INTRODUCTION

The effects of climate change have forced us to reduce our society's carbon footprint, increasing the environmental awareness of the population. There is no doubt that sustainable energy development is one of the biggest challenges in the world due to the ever-increasing energy demands to power everyday devices. Therefore, renewable energy sources and optimizing the efficiency during energy conversion processes are crucial for reducing the environmental impact of powering modern society. One way to maximize energy efficiency is through the electrical energy conversion of waste heat because more than 60% of global energy is lost as heat.[1] Thermoelectric materials generate an electrical potential from a temperature gradient through the Seebeck effect. Therefore, thermoelectric materials represent a direct way to harvest electricity in a safe, clean, and environmentally friendly manner.[2,3] The thermoelectric efficiency of a material is given by the dimensionless figure of merit, which is defined as

$$ZT = \frac{S^2\sigma}{\kappa}T \quad (1)$$

where S is the Seebeck coefficient of the thermoelectric material, σ and κ are the electrical and thermal conductivities, respectively, and T is the absolute temperature. To understand the dependence of thermoelectric efficiency with the parameters of eq 1, it is essential to highlight that S and σ depend on the electronic structure of each material. The thermal conductivity (κ) has two components, the contribution from charge carriers (κ_e) and lattice (κ_L), and, consequently, depends on the electronic structure and lattice dispersion relations (phonons).[4] ZT is used to compare materials with different thermal conductivities. However, to compare materials with similar thermal conductivities, the power factor (PF = $S^2\sigma$) is typically used.[5] Currently, thermoelectric applications are dominated by inorganic materials based on metallic alloys, such as Bi_2Te_3, Sb_2Te_3, PbTe, and SiGe, with ZT values around 2.6.[6−9] However, these inorganic materials present several environmental problems since they are mostly toxic and scarce, have a high production cost, and are difficult to process. Looking at this scenario, the thermoelectric community is looking for more sustainable alternatives that can overcome the mentioned drawbacks.[10]

Organic semiconductors such as conducting polymers represent an excellent alternative to traditional thermoelectric materials since they have low thermal conductivity and can achieve high electrical conductivity. Moreover, they are cost-competitive, lightweight, flexible, easy to produce, and large-

Received: June 1, 2022
Accepted: August 23, 2022
Published: September 6, 2022

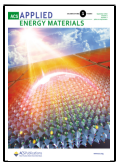

area processable.[11−15] Conducting polymers, in particular PEDOT (poly(3,4-ethylenedioxythiophene) doped with polystyrene sulfonic acid (PEDOT:PSS) is one of the most important conducting polymers because of its high electrical conductivity (800−2200 S cm^{-1}), relatively high Seebeck coefficient (18−80 $\mu V\ K^{-1}$), and low thermal conductivity (0.17−0.52 $W\ m^{-1}\ K^{-1}$).[16,17] Generally, conducting polymers are synthesized by wet chemistry methods, requiring time-consuming multistep procedures (i.e., synthesis, purification, and doping). Numerous research lines have been opened to improve their properties.[18−21] An exciting approach to modify the behavior of conducting polymers is by blending with other polymers to combine their properties to meet the needs of a given application. Typically, conducting polymers are blended with other polymers to tune the properties of the resulting film to satisfy the requirements of the final application.[22−24] These polymer blends can be prepared, for example, by spin-coating a solution of two polymers in a common solvent. This procedure is a straightforward method to approach new multicomponent functional materials. However, polymer blends generally lead to highly heterogeneous thin films with poor conductivity and optical and mechanical properties because of the propensity of polymers to phase-separate.[23,25]

In contrast, the in situ synthesis approach, where the conducting polymer is synthesized inside another polymer (used as a matrix), is a very promising strategy for combining the properties of both polymers. This multicomponent material is known as an interpenetrating polymer network (IPN).[26,27] Previous works reported a straightforward method to synthesize in situ polythiophenes into different host polymers through thermal annealing after spin-coating.[28,29] The resulting conducting polymer is, thus, entirely embedded into the host polymer when the polymerization takes place. As a result, homogeneous conducting polymer films are generated in a one step process. Furthermore, this approach allows one to combine the electrical properties of the in situ synthesized conducting polymer with the excellent film-forming properties of the host polymer.

Recently, we reported on the thermoelectric properties of PT-PMMA IPN thin film.[30] This synthetic approach allows the modification of the thermoelectric properties through the control of the polymerization process and the doping degree varying the oxidant salt/monomer molar ratio, showing electrical conductivities up to 20 S cm^{-1} and Seebeck coefficient of 110 $\mu V\ K^{-1}$. However, these films showed low PFs (18 $\mu W\ m^{-1}\ K^{-2}$).[30] A common approach to improve thermoelectric properties is using conducting polymers with nanostructured materials (carbon nanotubes, SnS, and Te, ...) to form a hybrid nanocomposite which produces an enhancement of the PF.[22−24,31−37] Despite the recent progress on increasing ZT in conducting polymers and their nanocomposites, further research is still needed to improve their efficiency to compete with traditional thermoelectric materials. Moreover, the synthesis and coating of hybrid nanocomposites remain challenging to obtain optimal thin films with enhanced thermoelectric properties. Therefore, the development of straightforward and low-cost synthetic routes is crucial for synthesizing hybrid thermoelectric materials for large-area fabrication of high-performance thermoelectric devices.

In this work, we report for the first time the simultaneous in situ synthesis of polythiophene (PT) and silver nanoparticles (Ag NPs) embedded in a PMMA matrix to form an IPN conducting polymer. The reaction is very fast and is carried out in a solid state during the thermal annealing after spin-coating. $AgClO_4$ is used as an oxidant for the oxidative polymerization of terthiophene (3T) and as a precursor of Ag NPs. The presence of Ag NPs significantly improves the electrical properties of the resulting IPN film. A complete understanding of the polymerization process of the 3T and the in situ synthesis of Ag NPs within the PMMA matrix is provided to optimize the conducting and thermoelectric properties. This approach allows us to design hybrid nanocomposite materials with high flexibility in terms of compositions and morphology and the possibility of optimizing and tuning the TE properties of the final film. In addition, the complete procedure is industrially scalable for large-area printing, representing a good opportunity for the thermoelectric industry to produce the next generation of TE materials and devices with a reduced cost.

EXPERIMENTAL SECTION

Materials. Terthiophene (3T, 99% purity), silver perchlorate, (1-methoxy-2-propyl) acetate (MPA), and poly(methyl methacrylate) (PMMA; average MW ∼ 996000) were purchased from Aldrich and used without further purification.

Synthesis of Ag-PT-PMMA Films. IPN films were prepared by the in situ polymerization of terthiophene (3T) by $AgClO_4$ inside the PMMA matrix. PMMA was used as a host polymer matrix because it can be easily processed into thin films utilizing different solvents by different deposition techniques. The polymerization of 3T results in polythiophene (PT) that provides electrical conductivity. Different amounts of 3T were dissolved in a solution of 4 wt % PMMA in MPA. Then, a specific amount of oxidant salt solution in MPA is added to obtain several Ag(I):3T molar ratios. The resulting solution is then spin-coated at 1800 rpm for 30 s onto a glass slide and a Si wafer slide for XPS and XRD measurements. The film was baked at different times at 160 °C. The thickness of the films was in the range of 75 and 125 nm, depending on the experimental conditions.

Characterization. The in situ polymerization of 3T was monitored by UV−vis−near-IR (UV−vis−NIR) spectroscopy using a JASCO V-770. Film thickness was measured by profilometry (Dektak 150 from Veeco). The film morphology was characterized by transmission electron microscopy (TEM) using a HITACHI HT7800 apparatus with 120 kV of high contrast, incorporating a CMOS EMSIS XAROSA digital camera of 20 Mpx.

The electric potential difference was measured with an Agilent 34401A multimeter, whereas the temperature difference was recorded with a Pt100 resistor connected to a Lakeshore 340 temperature controller. Four contacts were coated with silver paint on the film surface for electrical characterization. The electrical conductivity was measured with a Keithley 2400 source meter by using the Van der Pauw equation:[38]

$$e^{-\pi d R_1 \sigma} + e^{-\pi d R_2 \sigma} = 1 \tag{2}$$

where d is the thickness of the film, R_1 and R_2 are the electrical resistances along a vertical and horizontal edge, respectively, and σ is the electrical conductivity. The Seebeck coefficient was determined using a homemade apparatus composed of a Lakeshore 340 temperature controller and a Keithley 2750 multimeter/switching system. The Seebeck coefficient is obtained as the ratio of the electrical potential, ΔV, to the temperature difference, ΔT:

$$S = -\frac{\Delta V}{\Delta T} \tag{3}$$

The surface composition of IPN films was characterized by X-ray photoelectron spectroscopy (XPS) using an ESCALAB-210 ultrahigh-vacuum system from Thermo VG Scientific. Photoelectrons were excited using the Mg Kα line (1253.6 eV). The C 1s peak has been the reference of the binding energy (fixed to 285 eV). Grazing incidence X-ray diffraction (GIXRD) patterns were recorded by a

https://doi.org/10.1021/acsaem.2c01701
ACS Appl. Energy Mater. 2022, 5, 11067−11076

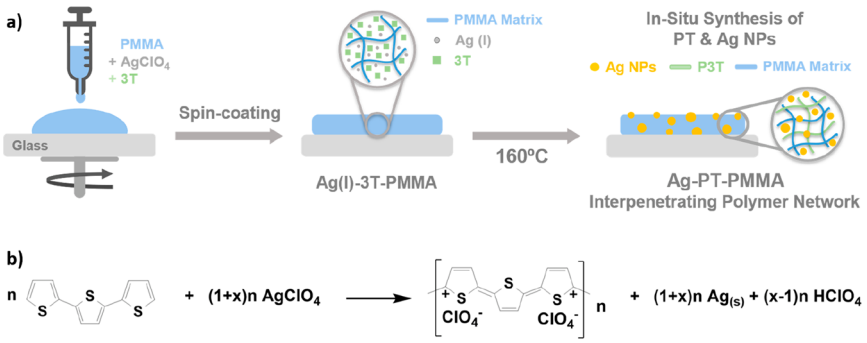

Figure 1. (a) Graphical illustration of the in situ synthesis of PT and Ag NPs embedded in PMMA matrix. (b) Oxidative polymerization of 3T by $AgClO_4$.

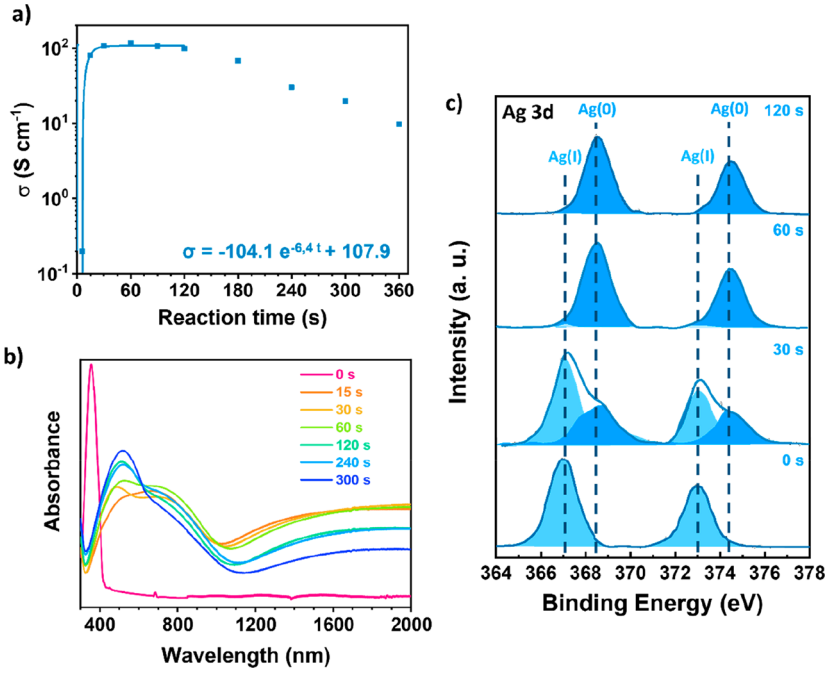

Figure 2. (a) Influence of the reaction time on the conductivity, σ, of Ag-PT-PMMA IPNs. (b) UV−vis−NIR spectra and (c) Ag 3d XPS spectra of an Ag-PT-PMMA IPN film as a function of reaction time. IPNs prepared at 22 wt % 3T in PMMA and a molar ratio $AgClO_4$:3T 2.8:1 at 160 °C.

Bruker D8 Advance X-ray diffractometer using Cu Kα radiation (λ = 0.15406 nm). Thermogravimetric analysis (TGA) was carried out using TA Instruments TGA550 equipment under an oxygen atmosphere. The sample was heated from 30 to 600 °C at a heating rate of 10 °C min^{-1}.

RESULTS AND DISCUSSION

Figure 1a shows the process for the in situ synthesis of the conducting IPN thin film. A precursor solution containing the reactants 3T, PMMA, and $AgClO_4$ is dropped in a glass substrate, spin-coated, and then heated. The in situ polymerization of 3T takes place within a PMMA polymeric matrix through an oxidative polymerization mechanism when $AgClO_4$ is used as an oxidizing agent. During the 3T polymerization, Ag(I) is reduced to Ag(0) and Ag NPs are simultaneously in situ generated. As a result, a conducting IPN thin film is synthesized in a single step by the oxidative polymerization of 3T (see Video S1 in the Supporting Information).

Figure 1b shows the oxidative polymerization reaction of 3T by $AgClO_4$. According to this, the coupling of two 3T molecules needs the reduction of two atoms of Ag(I) to Ag(0). Polymerization and doping occur simultaneously. Therefore, an extra amount of Ag(I) is necessary to partially oxidize the conjugated polymer and generate charge carriers (polarons and bipolarons).[5,39] The anion ClO_4^- from the oxidizing salt balances the charge to maintain the electroneutrality of the resulting polymer. In addition, ClO_4^- has a low nucleophilicity and is an essential factor that rules the polymerization and the doping.

Figure 2a shows the kinetics of the in situ polymerization of 3T. Here, the conductivity can be used to follow the extent of the polymerization reaction at 160 °C. The polymerization occurs very quickly inside PMMA. Experimental data can be fitted to an exponential equation, indicating that the kinetics is pseudo-first-order with a constant reaction rate of 6.4 s^{-1}. After only 15 s, the IPN already shows an electrical conductivity around 80 S cm^{-1}. The maximum conductivity (120 S cm^{-1}) is achieved after 60 s. Longer reaction times lead to a decrease in the electrical conductivity due to the overoxidation or decomposition of the PT, which affects the π-conjugated system, as discussed below.

The oxidative polymerization can also be followed by UV−vis−NIR spectroscopy, as shown in Figure 2b. During the

https://doi.org/10.1021/acsaem.2c01701
ACS Appl. Energy Mater. 2022, 5, 11067−11076

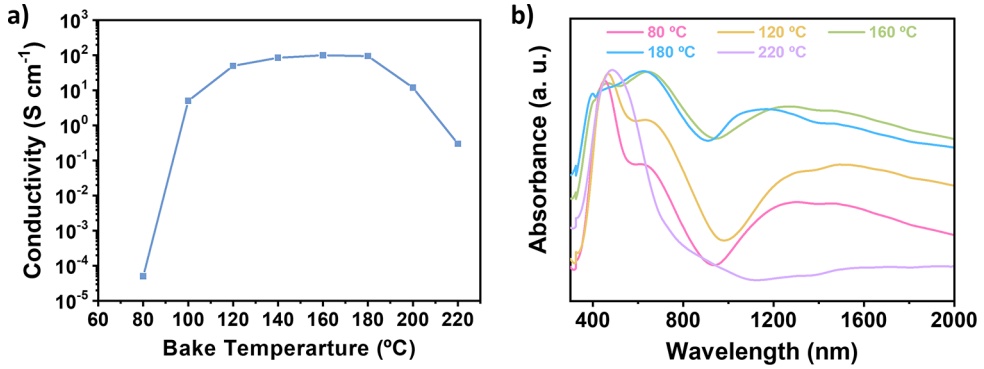

Figure 3. (a) Influence of the reaction temperature on electrical conductivity (σ) for Ag-PT-PMMA IPNs. (b) UV−vis−NIR spectra of a PT-PMMA IPN film as a function of reaction temperature. IPNs composition and conditions: 22 wt % 3T in PMMA and a molar ratio $AgClO_4$:3T 2.8:1 for 60 s.

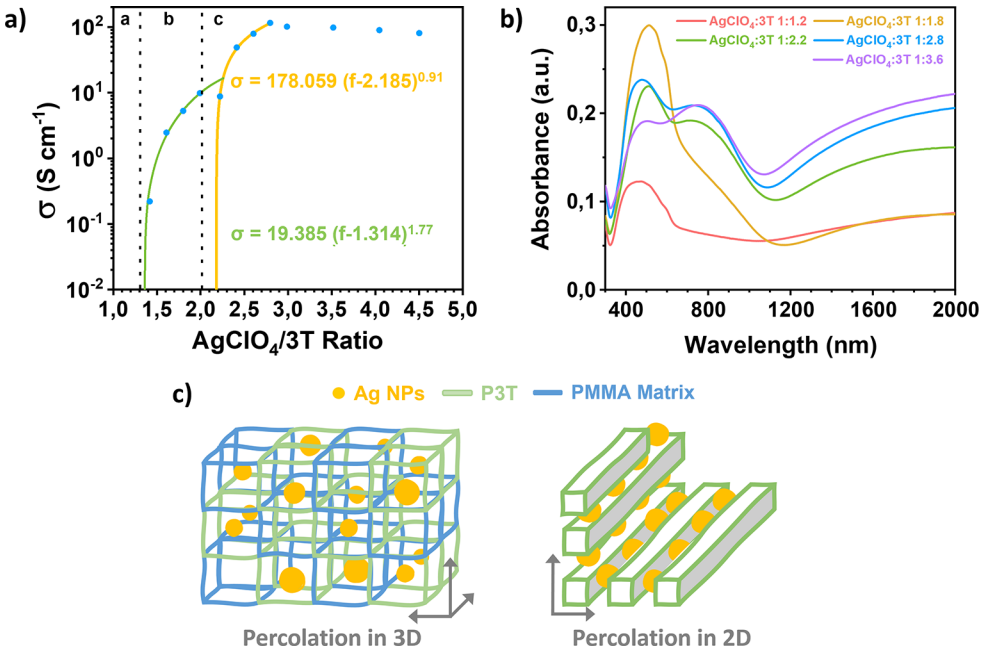

Figure 4. (a) Electrical conductivity, σ, of Ag-PT-PMMA IPN films as a function of the $AgClO_4$:3T molar ratio. Fitting equations to the experimental results are included according to the percolation theory. (b) UV−vis−IR spectra of different IPN films prepared from different $AgClO_4$:3T ratios. (c) Scheme of the proposed percolation in 2D and 3D dimensions for Ag-PT-PMMA IPNs.

thermal annealing, the thin film turns from colorless to yellowish and bluish (see Video S1 in the Supporting Information). During the thermal annealing, the colorless film turns yellow in a few seconds and then blue due to the oxidation (p-doping) of the PT chains.[5,39,40] PMMA and $AgClO_4$ are transparent in the UV−vis−NIR (300−2000 nm). Initially, the 3T-$AgClO_4$-PMMA films exhibited a maximum absorbance peak around 367 nm, corresponding to the $\pi-\pi^*$ band transition of the 3T. The oxidative coupling among 3T takes place with increasing reaction time, and the $\pi-\pi^*$ band transition red shifts toward 525 nm because the π-conjugation length increases.[41] As the polymerization takes place, Ag NPs are simultaneously synthesized. Ag NPs show a characteristic localized surface plasmon resonance (LSPR) band in the visible between 400 and 800 nm, depending on the size, shape, and aggregation of Ag NPs.[42−45] However, the LSPR band overlaps with the $\pi-\pi^*$ band transition of PT.[46,47] Simultaneously, we observe the bands of the polaronic (750 nm) and bipolaronic states (1400 nm) due to the partial oxidation of the PT by Ag(I), which leads to an increase in the doping level.[48,49] These three bands increase progressively with the reaction time as the 3T polymerization occurs, reaching a maximum absorbance after 60 s. The maximum electrical conductivity is also achieved after 60 s. Once this reaction time is exceeded, the polaronic and bipolaronic bands decrease, confirming the PT's overoxidation. Both the polaron and bipolaron bands dramatically decrease, leading to a substantial drop in conductivity. Consequently, the broad absorbance band located around 525 nm increases in intensity due to the degradation of PT by overoxidation and the synthesis of new Ag NPs.[50]

The synthesis of Ag NPs can be followed by X-ray photoelectron spectroscopy (XPS). Figure 2c shows the XPS spectra of 3T-$AgClO_4$-PMMA films for different polymerization times. Before reaction, we observe peaks of Ag $3d_{5/2}$ and Ag $3d_{3/2}$ of Ag(I) with a binding energy of 367 and 373 eV, respectively. After 30 s, two additional bands also appear at 368.4 and 374.4 eV due to Ag(0) in the form of Ag NPs.[51−53]

https://doi.org/10.1021/acsaem.2c01701
ACS Appl. Energy Mater. 2022, 5, 11067−11076

The presence of Ag(I) indicates that not all of the 3T has been polymerized to PT. After 60 s, the Ag(I) peaks decrease substantially, while Ag(0) peak increases noticeably. After 120 s, we only observe the peaks of Ag(0). XPS confirms that the reaction is very fast and $AgClO_4$ is quickly reduced to Ag NPs during the oxidative polymerization of 3T. The reaction needs only 60 s to be completed, in total agreement with UV−vis−NIR spectra and the conducting properties measured.

Figure 3 shows the influence of the reaction temperature on the in situ synthesis of Ag-PT-PMMA IPN thin films for 60 s. Even though the polymerization of thiophenes can take place at low temperatures,[54,55] the IPN's precursor solution is stable at room temperature, and the in situ polymerization initiates during the thermal annealing. Figure 3a shows the electrical conductivity of the film annealed from 80 to 220 °C. The conductivity at 80 °C is 5×10^{-5} S cm^{-1}. Below 80 °C, the IPN was too resistive (<10^{-7} S cm^{-1}) because the extent of polymerization is small to percolate into the PMMA matrix. From 80 to 180 °C, the conductivity increases by 6 orders of magnitude. Above 180 °C, the conductivity decreases with increasing temperature because PT is undergoing thermal degradation. These observations are confirmed with the UV−vis−NIR spectrum in Figure 3b. At low reaction temperatures, the band corresponding to the $\pi-\pi^*$ transition in PT has a higher intensity than the polaronic and bipolaronic bands, indicating a very low electrical conductivity. However, as the reaction temperature increases, the intensity of the polaronic and bipolaronic bands increases until a maximum value of 180 °C. This fact suggests that increasing the reaction temperature increases the PT chain's oxidation state (p-doping) and, therefore, the electrical conductivity of IPN film increases.[56,57] Above 180 °C, the polaronic and bipolaronic bands drop dramatically, indicating thermal degradation. As shown in TGA (Figure S1 in the Supporting Information (SI)), IPN films are stable until 220 °C. After this temperature, they start to lose weight.

Figure 4 shows the influence of the $AgClO_4$:3T molar ratio on the conducting properties of the IPN. The role of the $AgClO_4$:3T ratio is critical because it determines the concentration of PT, the charge carriers, and, therefore, the electrical conductivity and the Seebeck coefficient values.[56,57] The previous reaction conditions (60 s and 160 °C) have been used to study the effect of the different $AgClO_4$:3T molar ratios.

Following a characteristic percolation-type curve, the electrical conductivity increases with the $AgClO_4$:3T molar ratio. The conductivity of an IPN is related to the conducting polymer content in volume into the insulating host polymer and is based on the principles of the Percolation Theory given by[58]

$$\sigma = \sigma_0 (f - f_c)^t \tag{4}$$

where σ is the electrical conductivity, f is the volume of the conducting polymer in the film, f_c is the percolation threshold, σ_0 is a scaling factor, and t is the critical exponent. Percolation theory is frequently used to describe insulating-to-conductive transitions of materials based on conducting fillers and an insulating matrix. Generally, a low percolation threshold indicates a homogeneous distribution of the conducting polymer in the insulating host matrix. Therefore, this value has a notable effect on the morphology and electrical, mechanical, and thermal properties of properties of the IPN film.[28] On the other hand, the critical exponent in a percolation system is assumed to depend completely on the dimensionality of the lattice and is independent of the details of the lattice structure.[59] That is, for 3D systems, the critical exponent acquires values between 1.6 and 2.0, whereas, for 2D systems, the critical exponent varies between 1.1 and 1.3.[58] However, in electrically conducting percolated systems, the critical exponent does not follow the universal trend. In fact, conducting films based on insulating matrices with embedded conductive fillers and where the conduction process is controlled by tunnelling between fillers, the inverted Swiss-cheese model can be applied, which predicts t values between 0.8 and 1 for 2D systems and between 1.6 and 1.8 for 3D systems.[58,60]

The percolation threshold is determined by fitting experimental data to eq 4. Three regions can be clearly distinguished. At low $AgClO_4$:3T molar ratios (region a), the film's conductivity is low and the resistance cannot be measured. The percolation threshold is reached at 1.31 molar ratio (region b). At this point, enough PT chains are synthesized to contact each other to form an interconnected conducting network throughout the host insulating PMMA matrix. Above the percolation threshold from 1.4 to 2.0, the conductivity increases 2 orders of magnitude from 0.2 to 10 S cm^{-1}. Afterward, from 2.0 to 2.2, IPN conductivity reaches a plateau. Surprisingly, as the $AgClO_4$:3T molar ratio increases (region c), a second percolation curve is observed and electrical conductivity increases from 10 to 120 S cm^{-1}. The second percolation threshold is calculated to be 2.2. Finally, the highest conductivity is achieved for a molar ratio of 2.8.

Further increase in the molar ratio does not improve the conductivity. The UV−vis−NIR spectra support these results (Figure 4b), where the conjugated $\pi-\pi^*$ transition band (525 nm) decreases while polaronic (800 nm) and bipolaronic (1400 nm) bands increase as the $AgClO_4$:3T molar ratio increases due to a change in the oxidation state of the PT chains (stronger doping level).

Fitting the percolation curve allows for obtaining the percolating system's critical exponent. For example, from the fit of the first percolation curve (Figure 4a, green line), we obtained a t-value of 1.77, corresponding to percolation in 3D of the PT chains throughout the PMMA host matrix (Figure 4c). However, the second percolation curve (yellow line in Figure 4a) shows a t-value of 0.91, suggesting a percolation in 2D. In our previous work, when $Cu(ClO_4)_2$ was used as an oxidant agent, the resulting IPN film showed a single percolation with a t-value of 2.4 and a maximum conductivity (10 S cm^{-1}) lower than that of Ag-PT-PMMA (120 S cm^{-1}).[30] Below a value of 2.2 for the oxidant/monomer ratio, Cu(II)-PT-PMMA and Ag-PT-PMMA IPNs show similar conductivities. Therefore, we can assume that Ag NPs play a key role in the second percolation at high $AgClO_4$:3T ratios when the Ag content is high.

On the other hand, we can discard that Ag NPs percolates directly in the host polymer because the density of Ag (10.49 g cm^{-3}) is 1 order of magnitude higher than that of PMMA (1.18 g cm^{-3}) and PT (1.07 g cm^{-3}). Therefore, the percentage of the volume of Ag NPs in the final IPN is very low compared to PT and PMMA to percolate the IPN. Here, the 2D percolating system can be explained if we consider that the Ag NPs are located among PT chains to reduce the contact resistance between PT chains and enhance the charge transport, as shown in Figure 4c.[61] Accordingly, the IPN film

https://doi.org/10.1021/acsaem.2c01701
ACS Appl. Energy Mater. 2022, 5, 11067−11076

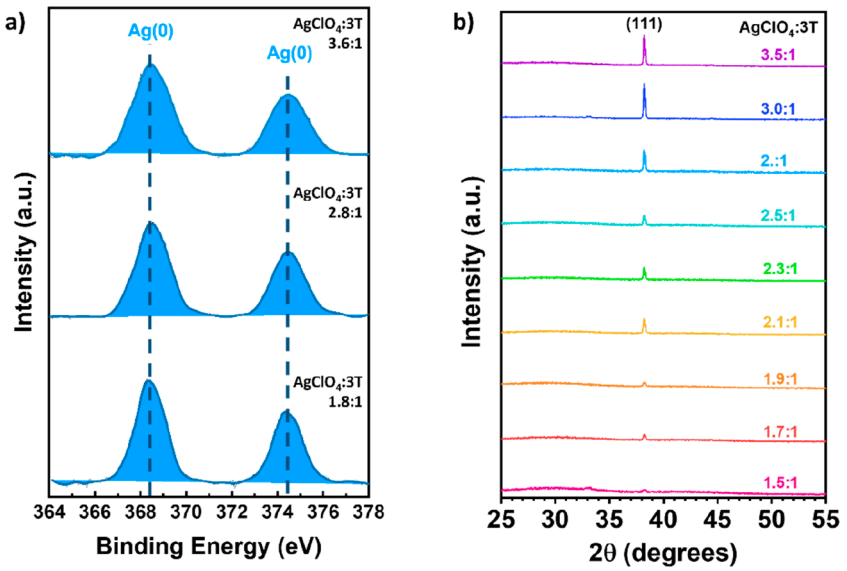

Figure 5. (a) XPS spectra of Ag(I)-3T-PMMA films measured in energy regions corresponding to the Ag 3d for three different Ag(I):3T ratios. (b) XDR spectra of Ag(I)-3T-PMMA films.

is obtained as a random distribution of the PT chains percolating PMMA in the 3D, while the Ag NPs are always distributed among PT chains to improve the charge transport.

Figure 5a shows XPS spectra of Ag(I)-3T-PMMA films measured in energy regions of Ag 3d for different Ag(I):3T ratios. XPS confirms that, after the oxidative polymerization of 3T, Ag(I) is reduced to Ag(0), as proposed in Figure 1b. Ag(0) shows the Ag $3d_{5/2}$ and $3d_{3/2}$ binding energies at 568.2 and 374.2 eV with a binding energy difference of 6 eV, indicating the formation of silver nanoparticles. This result agrees with the XRD spectra of Ag-PT-PMMA at different $AgClO_4$:3T ratios (Figure 5b). In addition, we observe a defined diffraction peak at 38.2°, increasing in intensity as the Ag(I):3T ratio increases. This diffraction peak is associated with the plane (111) of Ag face-centered-cubic structure (JCPDS File No. 4-0784).[62] The Scherrer equation shows that crystallite size increases with the Ag(I):3T ratio from 35.3 to 50.6 nm. Moreover, we observe a more intense peak for a higher Ag(I):3T ratio because more Ag NPs are in situ synthesized inside the PMMA matrix, confirmed by the peak area. Crystallite size and peak areas increase with the Ag(I):3T ratio, as shown in Table 1.

TEM images also confirm the presence of Ag NPs. Figure 6 shows the TEM images of Ag-PT-PMMA nanocomposite films synthesized at different $AgClO_4$:3T molar ratios. After the in situ polymerization of 3T inside PMMA, we can observe how Ag NPs are embedded inside a grayish matrix of PT-PMMA. The Ag NPs are well separated among them, but the conducting polymer is bridging the spacing between NPs. Furthermore, TEM images show the formation of larger particles from 40.5 to 61.6 nm as the Ag(I):3T ratio increases from 1.2 to 3.6. These results are in total agreement with the XRD analysis. SEM images of Ag-PT-PMMA films prepared from different Ag(I):3T molar ratios show a homogeneous surface (see Figure S2 in the SI). No phase segregation between PT and PMMA is observed, but surface roughness slightly increases with Ag(I):3T molar ratio.

Table 1. Crystallite Size, Silver Nanoparticle Size, and Peak Areas for Different Ag(I):3T Molar Ratios

ratio Ag(I):3T	crystallite size[a] (nm)	NP size[b] (nm)	peak area (111)
1.5	35.3	40.5	125.1
1.7	40.1	42.3	143.3
1.9	47.1	52.1	130.5
2.1	48.7	62.1	150.2
2.3	46.4	58.2	162.0
2.5	47.6	55.5	175.6
2.7	50.1	60.6	222.7
3.0	50.0	55.1	323.6
3.5	50.6	61.6	363.8

[a]Scherrer equation. [b]TEM.

Figure 7 shows the thermoelectric properties of the Ag-PT-PMMA films for different $AgClO_4$:3T molar ratios. As discussed earlier, the electrical conductivity significantly increases with the $AgClO_4$:3T ratio with a maximum of 120 S cm^{-1} at a 2.8 $AgClO_4$:3T ratio. Notice that the electrical conductivity has been depicted on a logarithmic scale. The general trend of the electrical conductivity with the molar ratio is a quick increase, in the logarithmic scale, with saturation around 2.8.

However, the values of the Seebeck coefficient follow a different trend. The Seebeck coefficient decreases from 66 to 52 $\mu V\ K^{-1}$ until an $AgClO_4$:3T molar ratio of 2.0. This trend is typically observed in conducting polymers, the Seebeck coefficient decreases as the conductivity increases, indicating the generation of more charge carriers (holes).[63]

In contrast, at larger $AgClO_4$:3T molar ratios, the Seebeck coefficient changes the trend and increases until values around 70 $\mu V\ K^{-1}$ due to a high amount of Ag NPs that have reached the percolation threshold. This fact is explained by improved carrier transport produced by the Ag NPs, allowing the Seebeck coefficient to increase without suppressing electrical conductivity, as shown in hybrid and nanocomposites based on conducting nanofillers.[64,65] This effect is inhibited by the overoxidation of the PT at higher $AgClO_4$:3T molar ratios (3.0), decreasing the Seebeck coefficient until 50 $\mu V\ K^{-1}$. A maximum power factor (PF = $S^2\sigma$) of 51 $\mu W\ m^{-1}\ K^{-2}$ was obtained for an $AgClO_4$:3T molar ratio of 2.8. This value is

https://doi.org/10.1021/acsaem.2c01701
ACS Appl. Energy Mater. 2022, 5, 11067−11076

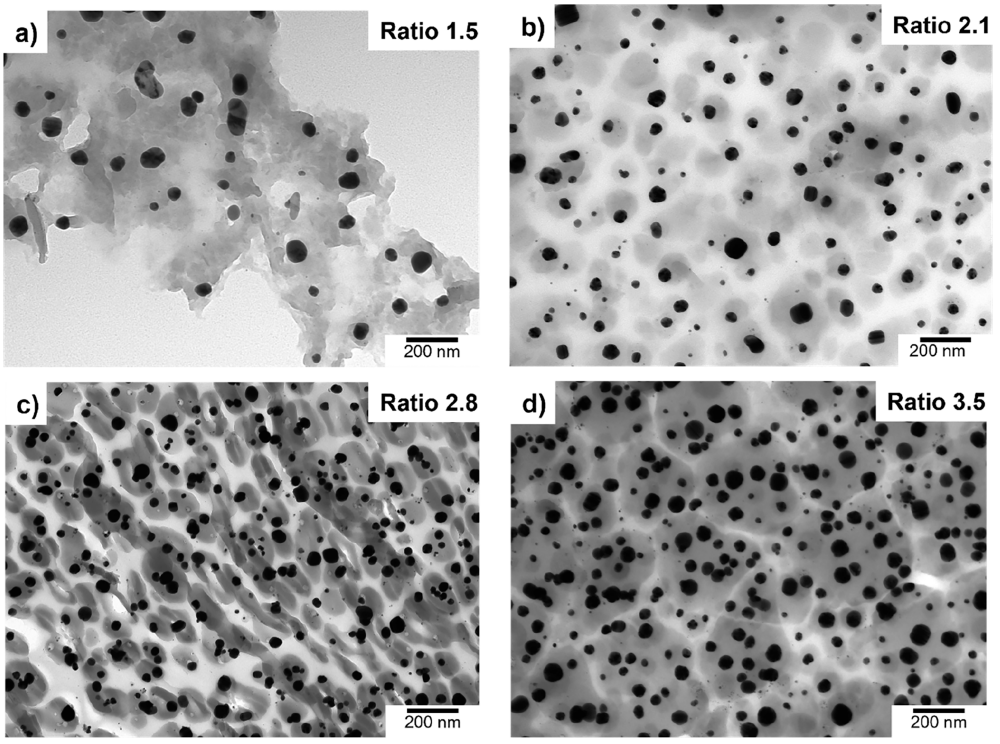

Figure 6. TEM images of Ag-PT-PMMA IPN films with different Ag(I):3T ratios (a) 1.5, (b) 2.1, (c) 2.8, and (d) 3.5.

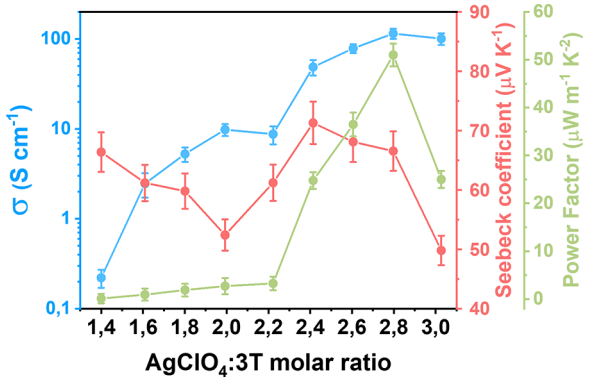

Figure 7. Electrical conductivity, σ, Seebeck coefficient, and power factor as a function of $AgClO_4$:3T molar ratio. Lines are used as a visual guide.

higher than previously reported ones for pure polythiophene films, which are around 10 μW m^{-1} K^{-2}.[66−69] These values are in the range of highly doped conducting polymers and nanocomposites.[70−72]

CONCLUSIONS

This study shows a straightforward synthetic route to obtain an interconnected polymeric network with thermoelectric applications. This route, based on the in situ polymerization of terthiophene with an oxidizing silver salt within a PMMA polymeric matrix, allows us to optimize the conducting and thermoelectric properties of the films. The polymerization and doping reaction takes place quickly, simultaneously, and after only 60 s achieving a maximum electrical conductivity of 120 S cm^{-1}. Ag NPs were in situ synthesized as a byproduct of the oxidative polymerization of 3T. The presence of Ag NPs was confirmed by the XPS, XRD, and SEM images. In addition, these Ag NPs influence the electrical conductivity, as shown in the percolation curve. At higher $AgClO_4$:3T molar ratios (>2.0:1), the Ag NPs start to percolate within the interconnected polymer network, increasing the electrical conductivity of the IPN by 1 order of magnitude. Finally, the thermoelectric properties of the optimized PT-Ag-PMMA film show two different trends for the Seebeck coefficients, decreasing at lower $AgClO_4$:3T molar ratios (<2.0:1) and increasing after this point due to the carrier filtering effect of the silver nanoparticles. A maximum power factor of 50 μW m^{-1} K^{-2} was obtained at an $AgClO_4$:3T molar ratio of 2.8:1, which is relatively high compared to thermoelectric materials based on an insulating polymer matrix.

ASSOCIATED CONTENT

Supporting Information

The Supporting Information is available free of charge at https://pubs.acs.org/doi/10.1021/acsaem.2c01701.

Additional thermal stability characterization of films (PDF)

Video S1 demonstrating of the film synthesis process (AVI)

AUTHOR INFORMATION

Corresponding Authors

Clara M. Gómez − *Institute of Materials Science (ICMUV), Universitat de València, 46980 Paterna, Spain*; Email: clara.gomez@uv.es

Rafael Abargues − *Institute of Materials Science (ICMUV), Universitat de València, 46980 Paterna, Spain*; orcid.org/0000-0001-5055-6339; Email: rafael.abargues@uv.es

https://doi.org/10.1021/acsaem.2c01701
ACS Appl. Energy Mater. 2022, 5, 11067−11076

Authors

José F. Serrano-Claumarchirant − *Institute of Materials Science (ICMUV), Universitat de València, 46980 Paterna, Spain*

Alvaro Seijas-Da Silva − *Institute of Molecular Science (ICMol), Universitat de València, 46980 Paterna, Spain*

Juan F. Sánchez-Royo − *Institute of Materials Science (ICMUV), Universitat de València, 46980 Paterna, Spain*; orcid.org/0000-0002-4005-0884

Mario Culebras − *Institute of Materials Science (ICMUV), Universitat de València, 46980 Paterna, Spain*

Andrés Cantarero − *Institute of Molecular Science (ICMol), Universitat de València, 46980 Paterna, Spain*; orcid.org/0000-0003-1999-4933

Complete contact information is available at: https://pubs.acs.org/10.1021/acsaem.2c01701

Author Contributions

§J.F.S.-C. and A.S.-D.S. contributed equally to this work.

Notes

The authors declare no competing financial interest.

■ ACKNOWLEDGMENTS

This research was supported by Spanish MINECO through Project a RTI2018-093711-B-I00 and the PROMETEO2020-016 from the Generalitat Valenciana. J.F.S.-C. acknowledges the financial support by the Spanish Ministry of Education and Vocational Training through the FPU Training (FPU17/01414) and Mobility (EST19/00037) Programs. R.A. acknowledge the support of Spanish MINECO through Retos de la Sociedad Project Nirvana (No. PID2020-119628RB-C31) by MCIN/AEI/10.13039/501100011033, the "Agència Valenciana de la Innovació" for the Valorització 2018 Project Hidronio (No. INNVAL10/18/032), and Valorització 2021 Project CATIOX (No. INNVA1/2021/56) and Spanish MINECO for his Ramón y Cajal Fellowship (No. RYC-2015-18349).

■ REFERENCES

(1) Forman, C.; Muritala, I. K.; Pardemann, R.; Meyer, B. Estimating the Global Waste Heat Potential. *Renewable and Sustainable Energy Reviews* **2016**, *57*, 1568−1579.

(2) Zhang, Q. H.; Huang, X. Y.; Bai, S. Q.; Shi, X.; Uher, C.; Chen, L. D. Thermoelectric Devices for Power Generation: Recent Progress and Future Challenges. *Adv. Eng. Mater.* **2016**, *18* (2), 194−213.

(3) Masoumi, S.; O'Shaughnessy, S.; Pakdel, A. Organic-Based Flexible Thermoelectric Generators: From Materials to Devices. *Nano Energy* **2022**, *92*, 106774.

(4) *Thermoelectrics Handbook: Macro to Nano*; Rowe, D. M., Ed.; CRC Press, Taylor & Francis Group: Boca Raton, 2006. DOI: 10.1201/9781420038903.

(5) Culebras, M.; Gómez, C. M.; Cantarero, A. Review on Polymers for Thermoelectric Applications. *Materials* **2014**, *7* (9), 6701−6732.

(6) Caballero-Calero, O.; Díaz-Chao, P.; Abad, B.; Manzano, C. V.; Ynsa, M. D.; Romero, J. J.; Rojo, M. M.; Martín-González, M. S. Improvement of Bismuth Telluride Electrodeposited Films by the Addition of Sodium Lignosulfonate. *Electrochim. Acta* **2014**, *123*, 117−126.

(7) Zhao, L.-D.; Lo, S.-H.; Zhang, Y.; Sun, H.; Tan, G.; Uher, C.; Wolverton, C.; Dravid, V. P.; Kanatzidis, M. G. Ultralow Thermal Conductivity and High Thermoelectric Figure of Merit in SnSe Crystals. *Nature* **2014**, *508* (7496), 373−377.

(8) Pei, Y.; Shi, X.; LaLonde, A.; Wang, H.; Chen, L.; Snyder, G. J. Convergence of Electronic Bands for High-Performance Bulk Thermoelectrics. *Nature* **2011**, *473* (7345), 66−69.

(9) Li, M.; Sun, Q.; Xu, S.; Hong, M.; Lyu, W.; Liu, J.; Wang, Y.; Dargusch, M.; Zou, J.; Chen, Z. Optimizing Electronic Quality Factor toward High-Performance Ge 1- x - y Ta x Sb y Te Thermoelectrics: The Role of Transition Metal Doping. *Adv. Mater.* **2021**, *33* (40), 2102575.

(10) Ao, D.; Liu, W.; Chen, Y.; Wei, M.; Jabar, B.; Li, F.; Shi, X.; Zheng, Z.; Liang, G.; Zhang, X.; Fan, P.; Chen, Z. Novel Thermal Diffusion Temperature Engineering Leading to High Thermoelectric Performance in Bi 2 Te 3 -Based Flexible Thin-Films. *Advanced Science* **2022**, *9* (5), 2103547.

(11) Orrill, M.; LeBlanc, S. Printed Thermoelectric Materials and Devices: Fabrication Techniques, Advantages, and Challenges. *J. Appl. Polym. Sci.* **2017**, *134* (3), 44256.

(12) Lee, S.; Kim, S.; Pathak, A.; Tripathi, A.; Qiao, T.; Lee, Y.; Lee, H.; Woo, H. Y. Recent Progress in Organic Thermoelectric Materials and Devices. *Macromol. Res.* **2020**, *28* (6), 531−552.

(13) Lindorf, M.; Mazzio, K. A.; Pflaum, J.; Nielsch, K.; Brütting, W.; Albrecht, M. Organic-Based Thermoelectrics. *Journal of Materials Chemistry A* **2020**, *8* (16), 7495−7507.

(14) Russ, B.; Glaudell, A.; Urban, J. J.; Chabinyc, M. L.; Segalman, R. A. Organic Thermoelectric Materials for Energy Harvesting and Temperature Control. *Nature Reviews Materials* **2016**, *1* (10), 16050.

(15) Hu, L.; Li, Z.; Zhou, Y.; Zhang, F.Conductive Polymers for Flexible Thermoelectric Systems. In *Flexible Thermoelectric Polymers and Systems*; John Wiley & Sons, 2022; pp 41−79, DOI: 10.1002/9781119550723.ch2.

(16) Xu, S.; Shi, X.-L.; Dargusch, M.; Di, C.; Zou, J.; Chen, Z.-G. Conducting Polymer-Based Flexible Thermoelectric Materials and Devices: From Mechanisms to Applications. *Prog. Mater. Sci.* **2021**, *121*, 100840.

(17) Culebras, M.; Choi, K.; Cho, C. Recent Progress in Flexible Organic Thermoelectrics. *Micromachines (Basel)* **2018**, *9* (12), 638.

(18) Luo, R.; Li, H.; Du, B.; Zhou, S.; Zhu, Y. A Simple Strategy for High Stretchable, Flexible and Conductive Polymer Films Based on PEDOT:PSS-PDMS Blends. *Org. Electron.* **2020**, *76*, 105451.

(19) Kee, S.; Kim, H.; Paleti, S. H. K.; el Labban, A.; Neophytou, M.; Emwas, A.-H.; Alshareef, H. N.; Baran, D. Highly Stretchable and Air-Stable PEDOT:PSS/Ionic Liquid Composites for Efficient Organic Thermoelectrics. *Chem. Mater.* **2019**, *31* (9), 3519−3526.

(20) Root, S. E.; Savagatrup, S.; Printz, A. D.; Rodriquez, D.; Lipomi, D. J. Mechanical Properties of Organic Semiconductors for Stretchable, Highly Flexible, and Mechanically Robust Electronics. *Chem. Rev.* **2017**, *117* (9), 6467−6499.

(21) Yang, Y.; Deng, H.; Fu, Q. Recent Progress on PEDOT:PSS Based Polymer Blends and Composites for Flexible Electronics and Thermoelectric Devices. *Materials Chemistry Frontiers* **2020**, *4* (11), 3130−3152.

(22) Goffri, S.; Müller, C.; Stingelin-Stutzmann, N.; Breiby, D. W.; Radano, C. P.; Andreasen, J. W.; Thompson, R.; Janssen, R. A. J.; Nielsen, M. M.; Smith, P.; Sirringhaus, H. Multicomponent Semiconducting Polymer Systems with Low Crystallization-Induced Percolation Threshold. *Nat. Mater.* **2006**, *5* (12), 950−956.

(23) McNeill, C. R.; Westenhoff, S.; Groves, C.; Friend, R. H.; Greenham, N. C. Influence of Nanoscale Phase Separation on the Charge Generation Dynamics and Photovoltaic Performance of Conjugated Polymer Blends: Balancing Charge Generation and Separation. *J. Phys. Chem. C* **2007**, *111* (51), 19153−19160.

(24) Smith, J.; Hamilton, R.; McCulloch, I.; Stingelin-Stutzmann, N.; Heeney, M.; Bradley, D. D. C.; Anthopoulos, T. D. Solution-Processed Organic Transistors Based on Semiconducting Blends. *J. Mater. Chem.* **2010**, *20* (13), 2562−2574.

(25) Nilsson, S.; Bernasik, A.; Budkowski, A.; Moons, E. Morphology and Phase Segregation of Spin-Casted Films of Polyfluorene/PCBM Blends. *Macromolecules* **2007**, *40* (23), 8291−8301.

(26) Sperling, L. H.*Interpenetrating Polymer Networks: An Overview*. In *Interpenetrating Polymer Networks*; Advances in Chemistry, Vol. *239*; American Chemical Society, 1994; pp 1−3. DOI: 10.1021/ba-1994-0239.ch001.
(27) Bansal, M.; Raos, B.; Aqrawe, Z.; Wu, Z.; Svirskis, D. An Interpenetrating and Patternable Conducting Polymer Hydrogel for Electrically Stimulated Release of Glutamate. *Acta Biomaterialia* **2022**, *137*, 124−135.
(28) Rodríguez-Cantó, P. J.; Martínez-Marco, M.; Sánchez-Royo, J. F.; Martínez-Pastor, J. P.; Abargues, R. In-Situ Synthesis of Thiophene-Based Multifunctional Polymeric Networks with Tunable Conductivity and High Photolithographic Performance. *Polymer (Guildf)* **2017**, *108*, 413−422.
(29) Abargues, R.; Nickel, U.; Rodríguez-Cantó, P. J. Charge Dissipation in E-Beam Lithography with Novolak-Based Conducting Polymer Films. *Nanotechnology* **2008**, *19* (12), 125302.
(30) Seijas-Da Silva, A.; Noguera-Gomez, J.; Rodríguez-Canto, P. J.; Sanchez-Royo, J. F.; Cantarero, A.; Gómez, C. M.; Abargues, R. In Situ Synthesis of Conducting Polymers: A Novel Approach toward Polymer Thermoelectrics. *J. Phys. Chem. C* **2020**, *124* (42), 22884−22892.
(31) Stevens, D. L.; Gamage, G. A.; Ren, Z.; Grunlan, J. C. Salt Doping to Improve Thermoelectric Power Factor of Organic Nanocomposite Thin Films. *RSC Adv.* **2020**, *10* (20), 11800−11807.
(32) Serrano-Claumarchirant, J. F.; Igual-Muñoz, A. M.; Culebras, M.; Collins, M. N.; Cantarero, A.; Gómez, C. M. Electrochemical Synthesis of Hybrid Layered Thermoelectric Materials Based on PEDOT/SnS Doped with Ag. *Advanced Materials Interfaces* **2021**, *8* (23), 2100951.
(33) Serrano-Claumarchirant, J. F.; Culebras, M.; Cantarero, A.; Gómez, C. M.; Muñoz-Espí, R. Poly(3,4-Ethylenedioxythiophene) Nanoparticles as Building Blocks for Hybrid Thermoelectric Flexible Films. *Coatings* **2020**, *10* (1), 22.
(34) Serrano-Claumarchirant, J. F.; Brotons-Alcázar, I.; Culebras, M.; Sanchis, M. J.; Cantarero, A.; Muñoz-Espí, R.; Gómez, C. M. Electrochemical Synthesis of an Organic Thermoelectric Power Generator. *ACS Appl. Mater. Interfaces* **2020**, *12* (41), 46348−46356.
(35) Jin, H.; Li, J.; Iocozzia, J.; Zeng, X.; Wei, P.-C.; Yang, C.; Li, N.; Liu, Z.; He, J. H.; Zhu, T.; Wang, J.; Lin, Z.; Wang, S. Hybrid Organic-Inorganic Thermoelectric Materials and Devices. *Angew. Chem., Int. Ed.* **2019**, *58* (43), 15206−15226.
(36) Culebras, M.; Igual-Muñoz, A. M.; Rodríguez-Fernández, C.; Gómez-Gómez, M. I.; Gómez, C.; Cantarero, A. Manufacturing Te/PEDOT Films for Thermoelectric Applications. *ACS Appl. Mater. Interfaces* **2017**, *9* (24), 20826−20832.
(37) Culebras, M.; Cho, C.; Krecker, M.; Smith, R.; Song, Y.; Gómez, C. M.; Cantarero, A.; Grunlan, J. C. High Thermoelectric Power Factor Organic Thin Films through Combination of Nanotube Multilayer Assembly and Electrochemical Polymerization. *ACS Appl. Mater. Interfaces* **2017**, *9* (7), 6306−6313.
(38) van der Pauw, L. J. A Method of Measuring Specific Resistivity and Hall Effect of Discs of Arbitrary Shape. *Philips Res. Rep.* **1958**, *13*, 1−9.
(39) Zozoulenko, I.; Singh, A.; Singh, S. K.; Gueskine, V.; Crispin, X.; Berggren, M. Polarons, Bipolarons, And Absorption Spectroscopy of PEDOT. *ACS Applied Polymer Materials* **2019**, *1* (1), 83−94.
(40) Harbeke, G.; Baeriswyl, D.; Kiess, H.; Kobel, W. Polarons and Bipolarons in Doped Polythiophenes. *Phys. Scr.* **1986**, *T13*, 302−305.
(41) Abargues, R.; Rodríguez-Cantó, P. J.; García-Calzada, R.; Martínez-Pastor, J. Patterning of Conducting Polymers Using UV Lithography: The in-Situ Polymerization Approach. *J. Phys. Chem. C* **2012**, *116* (33), 17547−17553.
(42) Abargues, R.; Gradess, R.; Canet-Ferrer, J.; Abderrafi, K.; Valdés, J. L.; Martínez-Pastor, J. Scalable Heterogeneous Synthesis of Metallic Nanoparticles and Aggregates with Polyvinyl alcohol. *New J. Chem.* **2009**, *33* (4), 913−917.
(43) Gradess, R.; Abargues, R.; Habbou, A.; Canet-Ferrer, J.; Pedrueza, E.; Russell, A.; Valdés, J. L.; Martínez-Pastor, J. P. Localized Surface Plasmon Resonance Sensor Based on Ag-PVA Nanocomposite Thin Films. *J. Mater. Chem.* **2009**, *19* (48), 9233.
(44) Abargues, R.; Albert, S.; Valdés, J. L.; Abderrafi, K.; Martínez-Pastor, J. P. Molecular-Mediated Assembly of Silver Nanoparticles with Controlled Interparticle Spacing and Chain Length. *J. Mater. Chem.* **2012**, *22* (41), 22204.
(45) Marqués-Hueso, J.; Abargues, R.; Valdés, J. L.; Martínez-Pastor, J. P. Ag and Au/DNQ-Novolac Nanocomposites Patternable by Ultraviolet Lithography: A Fast Route to Plasmonic Sensor Microfabrication. *J. Mater. Chem.* **2010**, *20* (35), 7436.
(46) Balan, L.; Malval, J.-P.; Lougnot, D.-J.In Situ Photochemically Assisted Synthesis of Silver Nanoparticles in Polymer Matrixes. In *Silver Nanoparticles*; Perez, D. P., Ed.; IntechOpen: Rijeka, Croatia, 2010. DOI: 10.5772/8504.
(47) Aghlara, H.; Rostami, R.; Maghoul, A.; SalmanOgli, A. Noble Metal Nanoparticle Surface Plasmon Resonance in Absorbing Medium. *Optik (Stuttg)* **2015**, *126* (4), 417−420.
(48) Culebras, M.; Gómez, C. M.; Cantarero, A. Enhanced Thermoelectric Performance of PEDOT with Different Counter-Ions Optimized by Chemical Reduction. *J. Mater. Chem. A* **2014**, *2* (26), 10109−10115.
(49) Shen, L.; Liu, P.; Liu, C.; Jiang, Q.; Xu, J.; Duan, X.; Du, Y.; Jiang, F. Advances in Efficient Polymerization of Solid-State Trithiophenes for Organic Thermoelectric Thin-Film. *Acs Applied Polymer Materials* **2020**, *2* (2), 376−384.
(50) Pluczyk, S.; Vasylieva, M.; Data, P. Using Cyclic Voltammetry, UV-Vis-NIR, and EPR Spectroelectrochemistry to Analyze Organic Compounds. *J. Visualized Exp.* **2018**, *140*, e56656.
(51) Behera, C.; Ghosh, S. P.; Kar, J. P.; Samal, S. L. Facile Synthesis and Enhanced Photocatalytic Activity of Ag-SnS Nanocomposites. *New J. Chem.* **2020**, *44* (27), 11684−11693.
(52) Gedi, S.; Minnam Reddy, V. R.; Reddy Kotte, T. R.; Kim, S. H.; Jeon, C. W. Chemically Synthesized Ag-Doped SnS Films for PV Applications. *Ceram. Int.* **2016**, *42* (16), 19027−19035.
(53) Jiang, Y.; Yang, Z.; Zhang, P.; Jin, H.; Ding, Y. Natural Assembly of a Ternary Ag-SnS-TiO2 Photocatalyst and Its Photocatalytic Performance under Simulated Sunlight. *RSC Adv.* **2018**, *8* (24), 13408−13416.
(54) Culebras, M.; Serrano-Claumarchirant, J. F.; Sanchis, M. J.; Landfester, K.; Cantarero, A.; Gómez, C. M.; Muñoz-Espí, R. Conducting PEDOT Nanoparticles: Controlling Colloidal Stability and Electrical Properties. *J. Phys. Chem. C* **2018**, *122* (33), 19197−19203.
(55) Serrano-Claumarchirant, J. F.; Culebras, M.; Muñoz-Espí, R.; Cantarero, A.; Gómez, C. M.; Collins, M. N. PEDOT Thin Films with N-Type Thermopower. *ACS Applied Energy Materials* **2020**, *3* (1), 861−867.
(56) Kim, D.; Zozoulenko, I. Why Is Pristine PEDOT Oxidized to 33%? A Density Functional Theory Study of Oxidative Polymerization Mechanism. *J. Phys. Chem. B* **2019**, *123* (24), 5160−5167.
(57) Imae, I.; Akazawa, R.; Harima, Y. Seebeck Coefficients of Regioregular Poly(3-Hexylthiophene) Correlated with Doping Levels. *Phys. Chem. Chem. Phys.* **2018**, *20* (2), 738−741.
(58) Nan, C.-W. Physics of Inhomogeneous Inorganic Materials. *Prog. Mater. Sci.* **1993**, *37* (1), 1−116.
(59) Sahimi, M.; Hughes, B. D.; Scriven, L. E.; Davis, H. T. Critical Exponent of Percolation Conductivity by Finite-Size Scaling. *Journal of Physics C: Solid State Physics* **1983**, *16* (16), L521−L527.
(60) Yoon, S.; Lee, S.-I. Possible Breakdown of the Universality of the Conductivity Critical Exponent in an Anisotropic Percolation System. *Physica B: Condensed Matter* **1990**, *167* (2), 133−137.
(61) Zhang, R.; Moon, K.; Lin, W.; Wong, C. P. Preparation of Highly Conductive Polymer Nanocomposites by Low-Temperature Sintering of Silver Nanoparticles. *J. Mater. Chem.* **2010**, *20* (10), 2018.
(62) Aznar-Gadea, E.; Rodríguez-Canto, P. J.; Martínez-Pastor, J. P.; Lopatynskyi, A.; Chegel, V.; Abargues, R. Molecularly Imprinted Silver Nanocomposites for Explosive Taggant Sensing. *ACS Applied Polymer Materials* **2021**, *3* (6), 2960−2970.

(63) Zhao, W.; Ding, J.; Zou, Y.; Di, C.; Zhu, D. Chemical Doping of Organic Semiconductors for Thermoelectric Applications. *Chem. Soc. Rev.* **2020**, *49* (20), 7210−7228.
(64) Cho, C.; Culebras, M.; Wallace, K. L.; Song, Y.; Holder, K.; Hsu, J.-H.; Yu, C.; Grunlan, J. C. Stable N-Type Thermoelectric Multilayer Thin Films with High Power Factor from Carbonaceous Nanofillers. *Nano Energy* **2016**, *28*, 426−432.
(65) Culebras, M.; Ren, G.; O'Connell, S.; Vilatela, J. J.; Collins, M. N. Lignin Doped Carbon Nanotube Yarns for Improved Thermoelectric Efficiency. *Advanced Sustainable Systems* **2020**, *4* (11), 2000147.
(66) Hiraishi, K.; Masuhara, A.; Nakanishi, H.; Oikawa, H.; Shinohara, Y. Evaluation of Thermoelectric Properties of Polythiophene Films Synthesized by Electrolytic Polymerization. *Jpn. J. Appl. Phys.* **2009**, *48* (7), 071501.
(67) Huner, K.; Karaman, F. The Effect of External Magnetic Field on the Thermoelectric Properties of Polythiophene. *Materials Research Express* **2019**, *6* (1), 015302.
(68) Imae, I.; Koumoto, T.; Harima, Y. Thermoelectric Properties of Polythiophenes Partially Substituted by Ethylenedioxy Groups. *Polymer (Guildf)* **2018**, *144*, 43−50.
(69) Yao, W.; Shen, L.; Liu, P.; Liu, C.; Xu, J.; Jiang, Q.; Liu, G.; Nie, G.; Jiang, F. Electrochemical Doping Engineering Tuning of the Thermoelectric Performance of a π-Conjugated Free-Standing Poly(Thiophene-Furan) Thin-Film. *Mater. Chem. Front.* **2020**, *4* (2), 597−604.
(70) Kiefer, D.; Kroon, R.; Hofmann, A. I.; Sun, H.; Liu, X.; Giovannitti, A.; Stegerer, D.; Cano, A.; Hynynen, J.; Yu, L.; Zhang, Y.; Nai, D.; Harrelson, T. F.; Sommer, M.; Moulé, A. J.; Kemerink, M.; Marder, S. R.; McCulloch, I.; Fahlman, M.; Fabiano, S.; Müller, C. Double Doping of Conjugated Polymers with Monomer Molecular Dopants. *Nat. Mater.* **2019**, *18* (2), 149−155.
(71) Jacobs, I. E.; Moulé, A. J. Controlling Molecular Doping in Organic Semiconductors. *Adv. Mater.* **2017**, *29* (42), 1703063.
(72) Untilova, V.; Biskup, T.; Biniek, L.; Vijayakumar, V.; Brinkmann, M. Control of Chain Alignment and Crystallization Helps Enhance Charge Conductivities and Thermoelectric Power Factors in Sequentially Doped P3HT:F4TCNQ Films. *Macromolecules* **2020**, *53* (7), 2441−2453.

NOTE ADDED AFTER ASAP PUBLICATION

After this paper was published ASAP September 6, 2022, punctuation errors in the third author's name were corrected. The revised version was reposted September 7, 2022.

https://doi.org/10.1021/acsaem.2c01701
ACS Appl. Energy Mater. 2022, 5, 11067−11076